

# Extraction of triplicated PKP phases from noise correlations

Han H. Xia,<sup>1</sup> Xiaodong Song<sup>1,2</sup> and Tao Wang<sup>1</sup>

<sup>1</sup> Institute of Geophysics and Geodynamics, School of Earth Sciences and Engineering, Nanjing University, Nanjing 210093, China.

E-mail: [xsong@illinois.edu](mailto:xsong@illinois.edu)

<sup>2</sup> Department of Geology, University of Illinois at Urbana-Champaign, Champaign, IL 61801, USA

Accepted 2016 January 11. Received 2016 January 10; in original form 2015 August 21

## SUMMARY

Ambient noise correlation method has been widely used to extract surface waves and tomography. The extraction of body waves has been very limited, but recent reports have suggested promises for deep incident waves. Here we report our first observations of triplicated PKP phases (important phases for studying the Earth's core) and confirm observations of other body-wave core phases from noise correlations. We use dense seismic arrays in South America and China Regional Seismic Networks at distances from 145° to the antipode. We can clearly observe different PKP branches (df, bc and ab) in stacks of the station–station correlations. Both ambient noise and earthquake coda contribute to PKP phases. However, the contributions vary with frequency and with body-wave phases. At shorter periods (5–20 s), three branches of PKP (df, bc and ab) can be extracted from ambient noise and the ab phase from earthquake coda. At longer periods (15–50 s), earthquake coda are effective in generating the df branch, but not the ab branch. The generation of the PKIKP phase (df branch) from earthquake coda does not depend on earthquake focal mechanisms or focal depths. However, earthquakes far from the stations contribute more than events closer by. The best coda window is around 10 000–40 000 s and the best magnitude threshold is  $M_w$  greater than 6.8 or 6.9. The observation of triplicated PKP branches from noise correlations provides a new type of data for studying the Earth's deep interior, in particular the inner core anisotropy, which overcomes some of the limitations of traditional earthquake-based studies (such as limited source distributions and source location errors).

**Key words:** Noise correlation; PKP triplication; Inner core; Body waves.

## 1 INTRODUCTION

During the last decade, ambient noise correlation has been widely used in studying the structure of our planet (e.g. Shapiro *et al.* 2005; Yao *et al.* 2006; Zheng *et al.* 2008) since the early works on the extraction of the empirical Green's function (EGF) between receivers from noise correlation (Lobkis & Weaver 2001; Campillo & Paul 2003; Shapiro & Campillo 2004). So far, most studies have focused on surface waves, which are easily extracted from ambient noise correlations. However, some studies have shown it feasible to extract signals of body waves from ambient noise correlations (Roux *et al.* 2005; Zhan *et al.* 2010; Poli *et al.* 2012; Boué *et al.* 2013; Lin & Tsai 2013; Lin *et al.* 2013; Nishida 2013). Stacking EGFs between the USArray stations across the continental U.S. Lin *et al.* (2013) reported observations of many body wave phases sampling the Earth's core, including PKIKP<sup>2</sup> (P wave traversing the inner core and bounced back from the other side of the globe). Using near antipodal stations around the globe, Lin & Tsai (2013) reported additional body waves (including antipodal PKIKP waves)

from individual station pairs without stacking. In a global survey, Boué *et al.* (2013) and Nishida (2013) showed that various body waves through the entire Earth can be extracted from the seismic noise. More recently, Wang *et al.* (2015) showed robust observations of PKIKP<sup>2</sup> and PKIIPK<sup>2</sup> phases (which have never been observed simultaneously from an earthquake) from stacks of autocorrelations at global arrays using earthquake coda. The source for the generation of the body waves is under debate, which is suggested to come from the coda of large earthquakes (Lin & Tsai 2013; Lin *et al.* 2013; Wang *et al.* 2015), or from the ambient noise (Boué *et al.* 2013; Nishida 2013). Furthermore, Boué *et al.* (2014) suggested that certain phases (in particular, core phases ScS, PKIKP) reconstructed at long periods (25–100 s) come from reverberation of earthquakes waves and there are spurious arrivals. At short period (5–10 s), the reconstructed phases (e.g. P, SS) are not correlated with seismicity, which suggest the influence of the scattering of the wavefield rather than wave reverberation.

Multiple PKP core phases arise from the P velocity decrease at the core–mantle boundary and velocity increase at the inner

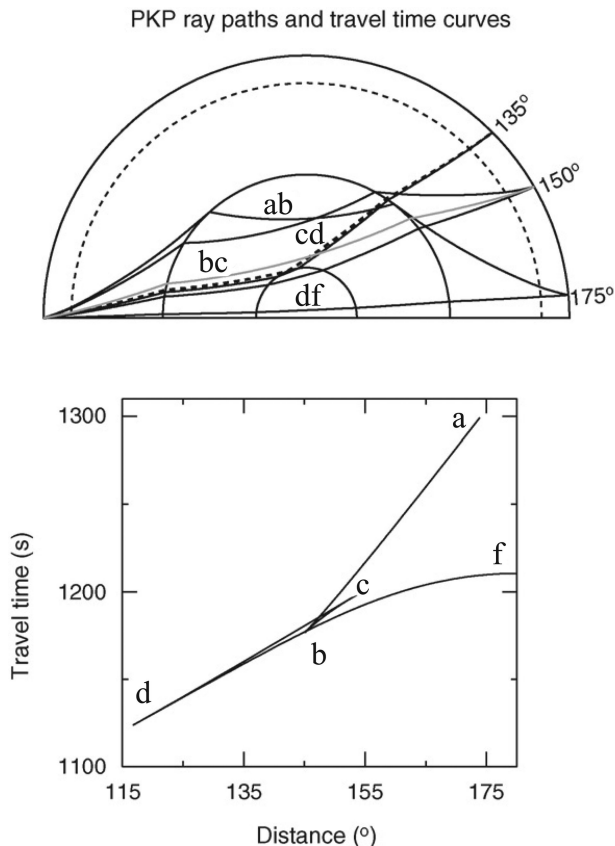


**Figure 1.** PKP ray paths and travelttime curves. Three PKP branches (df, bc and ab) of PKP waves from about  $150^\circ$  to  $180^\circ$  are extracted from noise correlations in this study.

core boundary, which are commonly observed from earthquakes (Fig. 1). They include the PKIKP (or PKPdf) phase that traverses the inner core, the PKiKP (or PKPcd) that is reflected from the inner core boundary, the PKPbc phase that turns at the bottom of the outer core and the PKPab phase that turns at the mid-outer core. PKP waveforms and differential travel times between branches are powerful in studying the structure of the Earth's core, which reduce influences from earthquake sources and mantle heterogeneities. They have been extensively used to study the Earth's inner core such as anisotropy (e.g. Shearer & Toy 1991; Creager 1992; Song & Helmbberger 1993), rotation (e.g. Song & Richards 1996; Vidale *et al.* 2000; Zhang *et al.* 2005), attenuation (e.g. Cormier *et al.* 1998), hemispherical structure (e.g. Tanaka & Hamaguchi 1997; Niu & Wen 2001), 3D structure (e.g. Sun & Song 2008a; Irving & Deuss 2011), inner core boundary topography (e.g. Wen 2006; Cao *et al.* 2007; Song & Dai 2008) and inner(most) inner core (e.g. Ishii & Dziewoński 2002; Sun & Song 2008b).

In this study, we report observations of triplicated PKP phases in stacked EGFs from noise correlations. We also explore possible noise sources for the generation of the core phases and factors affecting the quality of the phases and parameters for enhancing the signal-to-noise ratios (SNRs).

## 2 DATA AND METHOD

We used 4 yr of continuous data (long-period vertical component) from January 2008 to December 2011 with a total of 1017 stations

from the China Regional Seismic Networks (Zheng *et al.* 2009) and 310 portable South America (SA) stations from IRIS DMC (Fig. 2). The distances between SA and Chinese stations span from  $145^\circ$  to  $180^\circ$ . The distance range is ideal for observing three branches of PKP (df, bc and ab) between  $147^\circ$  and  $160^\circ$  and df and ab branches between  $160^\circ$  to  $180^\circ$  (Fig. 1).

The continuous data at each station were stored in 1-d segments. They were used in several ways, including all the continuous data available, segments of the days when earthquakes of certain magnitude occurred, or portions of records after major earthquakes (earthquake coda). We followed the basic procedure similar to Bensen *et al.* (2007) to compute the EGFs between stations. The data-preprocessing procedure included band-pass filtering (between 5 and 50 s, unless noted otherwise) and spectral whitening. We used a time-domain normalization with a running absolute mean to reduce the effect of energetic sources (such as earthquakes). Only the symmetric part of the EGF is used, which is obtained by folding and stacking the positive and negative time lags of the EGF.

## 3 RESULTS

### 3.1 Observations triplicated PKP phases

We used only a subset of station–station pairs with azimuths between  $30^\circ$  to  $110^\circ$  (originating from the SA side) and distances between  $145^\circ$  and  $180^\circ$ . This azimuthal range contains the densest station pairs covering a wide distance range. Due to the low SNR in the EGF of a single station pair, we stacked EGFs within  $0.5^\circ$  to enhance SNRs of body waves. In this study, the SNR is defined as the peak amplitude of the PKIKP phase divided by the root mean square of 0 to 500 s lag time of cross-correlation where there are no obvious signal arrivals.

The EGF stacks show clearly many body wave phases (Fig. 3), including PKIKP (PKPdf), PKPab, PP, PKPPcP and SKSP. Some of the phases (PKIKP, PP, PKPPcP and SKSP) have been reported earlier (Boué *et al.* 2013; Lin & Tsai 2013; Nishida 2013). All of these phases except PKIKP show, to varying degrees, arrivals along the minor arc and the major arc of the great circle path when the station pair is away from the exact antipode. The arrival times of these phases and the slopes of the arrival times with respect to distance, along minor or major arcs, are consistent with predictions for a 1-D global reference model IASP91 (Kennett & Engdahl 1991) for a surface source.

The most interesting observation is the triplicated PKP phases across distance range from less than  $150^\circ$  to  $180^\circ$ , which are clearly shown in the enlarged time window (1150–1350 s) (Fig. 4). Such triplicated arrivals have been not reported before from noise correlations. At smaller distances ( $145^\circ$  to  $160^\circ$  or so), we can even see three branches of PKP (df, bc and ab). Beyond  $160^\circ$ , we can see the df and ab branches consistently to the antipodal distance. The absolute arrival times as well as the relative travel times between difference branches are in general agreement with predictions for a 1-D reference model.

### 3.2 Noise sources for the generation of PKP waves

As mentioned above, the sources generating the body waves are uncertain. It has been suggested to come from the coda of large earthquakes (Lin & Tsai 2013; Lin *et al.* 2013), from the ambient noise (Boué *et al.* 2013; Nishida 2013), which could be

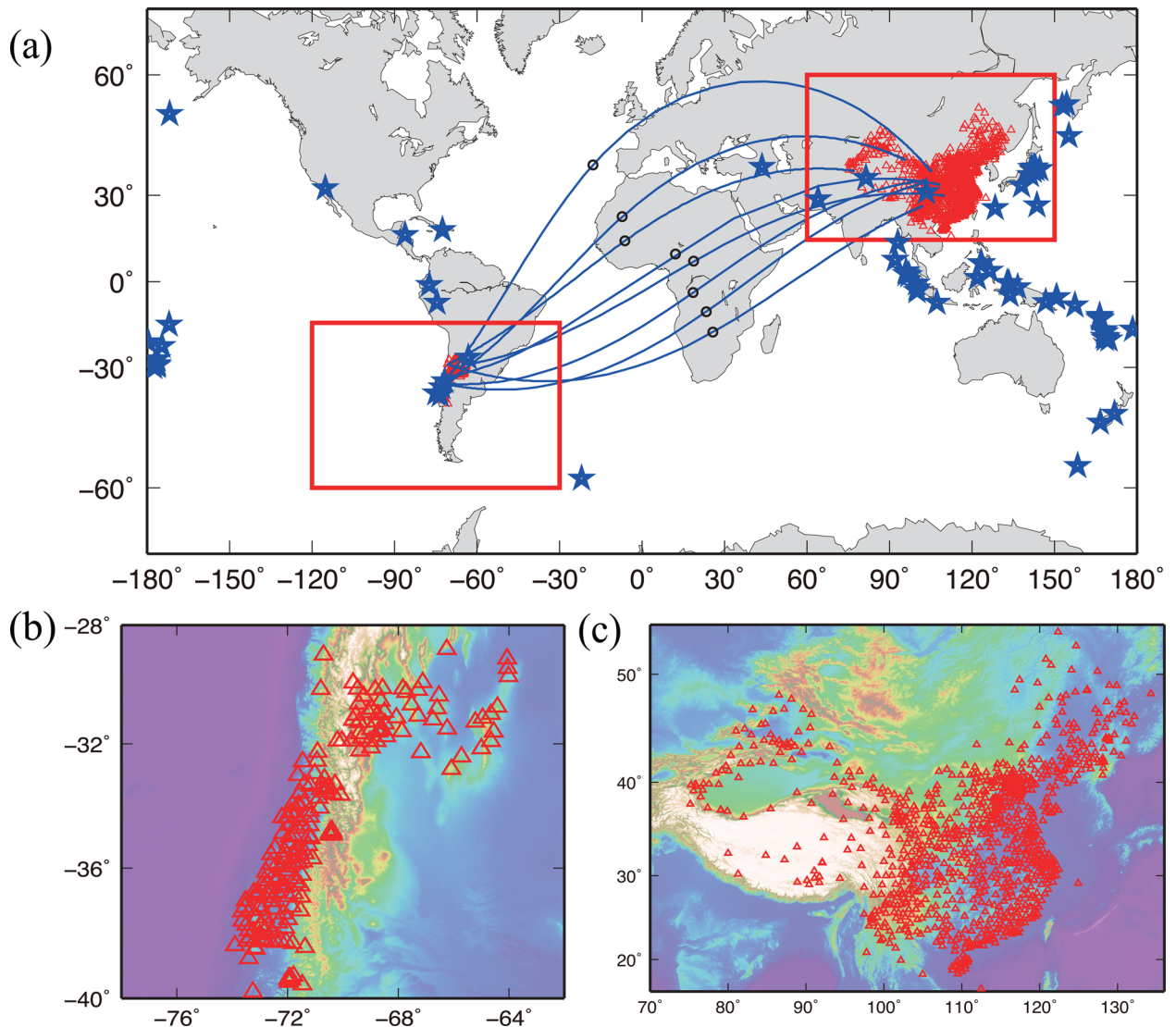


**Figure 2.** Maps of seismic stations (red triangles in panels a–c) in South America (SA) (b) and China (c) used in this study. Shown also in panel (a) are major earthquakes ( $M_w \geq 7.0$ , blue stars) and selected great circle paths (blue lines, in azimuths of  $30^\circ$  to  $110^\circ$  from SA stations to stations in China used in Section 3.1) and turning points of the ray paths (black circles).

frequency-dependent (Boué *et al.* 2014). Below we explore possible noise sources for the generation of the PKP phases and factors affecting the observations of the phases and parameters for enhancing the SNRs.

### 3.2.1 Influences of noise sources on the SNR of PKP

We conducted various tests to explore the influences of the noise sources from various earthquakes on the EGFs by using only the time segments selected based on earthquake parameters (Figs 5 and 6). We selected a small interstation distance range between  $170^\circ$  and  $170.5^\circ$ . In this distance range, we have the densest sample with the most number of station pairs (a total of 607 pairs) within the  $0.5^\circ$  interval. The dense coverage would make sure that we obtain a sufficiently large SNR of the body waves when a subset of the data is selected in order to make meaningful comparison with different selection criteria. In comparison with the ini-

tial computation based on ambient noise correlations, we explore data selections based on earthquake magnitude, location and focal mechanisms.

First, we examine earthquake magnitude and select days when there is an earthquake above a certain magnitude threshold. Lin & Tsai (2013) suggested that the coda energy between around 10 000 to 30 000 s after a large earthquake contributes a majority of the signal in the noise correlation. Here we also focus on the segments containing earthquake coda. If an earthquake occurs after 18th hour from the start of the day, we select the next day of data so that the majority of the contributing coda is included. Originally, without imposing any data selection criteria, we have a total number of  $N = 1461$  d of continuous data. The magnitude thresholds we selected are  $M_w \geq 6.0$  ( $N = 407$ ),  $M_w \geq 7.0$  ( $N = 52$ ) and  $M_w \geq 8.0$  ( $N = 3$ ), respectively. Although the number of days differ greatly, the SNRs of the PKIKP waves are all high, which are 6.63 when all the data (continuous ambient noise data) are used, 5.96 for  $M_w \geq 6.0$  and 7.26 for  $M_w \geq 7.0$ , respectively (traces 1–3 in

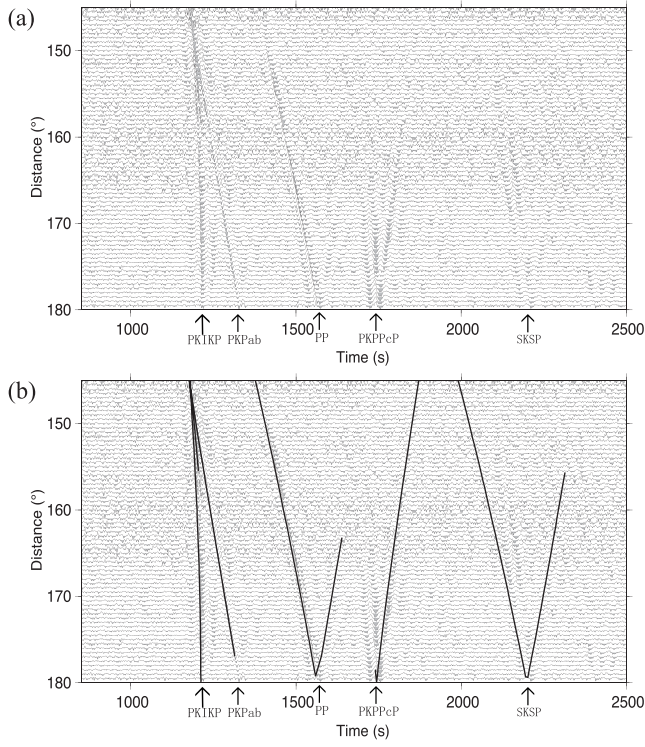


**Figure 3.** Stacks of empirical Green's functions (EGFs) from station–station correlations within  $0.5^\circ$  interval for each stack. Panel (b) is the same as panel (a) but with the theoretical arrival times (black dashed lines) for the IASP91 model. The separate panels show better the body-wave arrivals.

Fig. 5). The result demonstrates that major source of the coherent energy for PKIKP phase is generated by big earthquakes. The higher SNR for  $M_w \geq 7.0$  with fewer days, in comparison with that for  $M_w \geq 6.0$  with more days, suggests that large earthquakes contribute more than smaller ones. The fluctuation of the SNRs for these cases also suggests that the contribution from individual earthquakes may vary. If we use only days with  $M_w \geq 8.0$  (trace 4 in Fig. 5, with only 3 d of available data), the SNR is relatively low (2.94) but some phases (PKIKP and PKPPcP) are still observable. Note different phases are affected differently, for example, the PP phases in traces 4 and 5 are much poorer (not visible) than in traces 1 and 2.

Second, we examine the effect of earthquake focal mechanisms on the body-wave retrievals (traces 5 and 6 in Fig. 5). We use  $M_w \geq 6.0$  earthquakes and divide them into two groups, predominantly strike-slip (slip within  $45^\circ$  of the strike or its opposite direction) and predominantly dip-slip (slip within  $45^\circ$  of the up- or downdip direction). The two groups have similar number of days of data and the SNRs of the PKIKP waves from these two groups are also similar. However, the PKIKP waveforms show notable difference, indicating that the radiations of the energy from different types of earthquakes may affect distribution of the noise source, although they all contribute to the convergence of the EGFs.

Third, we examine the effect from earthquake depth and distribution (using  $M_w \geq 6.0$  earthquakes). Stacks of the EGFs with days that contain deep ( $\geq 50$  km) and shallow ( $< 50$  km) earthquakes, respectively, can produce body-wave signals similarly, suggesting that both deep and shallow earthquakes con-

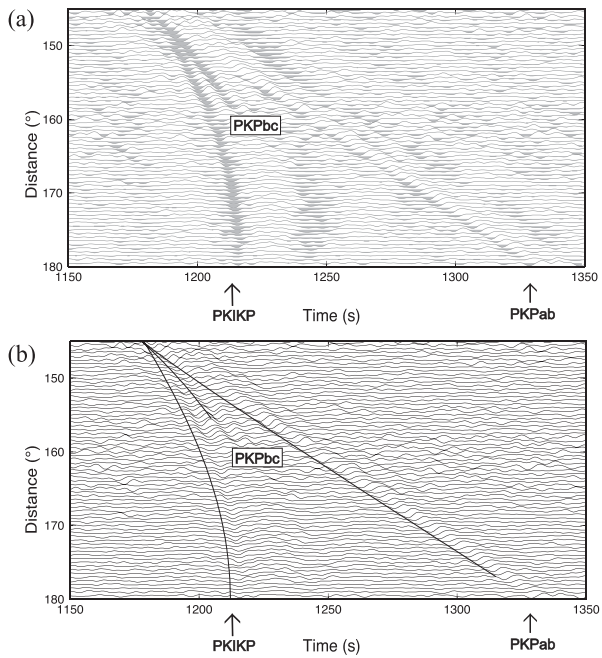


**Figure 4.** Enlarged views of stacked EGFs showing triplicated PKP phases. The theoretical arrival times of PKIKP, PKPbc and PKPab (black dashed lines in panel b) are computed for the IASP91 model. Note that the ab phase has a  $180^\circ$  phase shift, which shows up in the difference of the highlighted waveforms relative to those of the df and bc phases in panel (a).

tribute to the energy responsible for the convergence of the body waves.

We have also examined the effect of earthquake locations ( $M_w \geq 6.0$ ) relative to the stations (Fig. 6). We separate the earthquakes into three groups, earthquakes that are close to the two centres of the station groups in China and SA ( $\leq 35^\circ$ , labelled as the ‘near’ group); those that are further away from the two centres ( $> 60^\circ$ , the ‘far’ group) and those in the intermediate distances ( $> 35^\circ$  and  $\leq 60^\circ$ , the ‘intermediate dist’ group). The numbers of earthquakes in each group are roughly the same. We see that the SNRs of the body waves from the ‘near’ group (SNR = 4.96, trace 1 in Fig. 6b) and the ‘intermediate dist’ group (SNR = 5.74, trace 2 in Fig. 6b) are much lower than that from the ‘far’ group (SNR = 7.93, trace 3 in Fig. 6b). Therefore, our result suggests that the position of earthquakes relative to stations plays an important role in extracting core phases from interstation correlations. We separate further the earthquakes in the ‘far’ and ‘intermediate dist’ groups into three groups according to the azimuths relative to the great-circle path between the two centres: (1) ‘in-line’ (trace 4 in Fig. 6b); (2) ‘intermediate azimuths’ (trace 5 in Fig. 6b); 3) and ‘off-line’ (trace 6 in Fig. 6b). The decreasing trend in the SNRs from the ‘in-line’ to the ‘off-line’ groups, despite the increasing numbers of earthquakes, suggests that the ‘in-line’ earthquakes contribute more energy to the core phases, even though earthquakes at other azimuths contribute too. Recently, Sens-Schönenfelder *et al.* (2015) found that the late earthquake coda waves are not equipartitioned, implying that teleseismic body waves can only be extracted from the coda when the earthquake and the receivers are located on a great circle. Our results above are consistent with their conclusion, however, the earthquakes from off-great circle appear to contribute also to the convergence of the EGFs.

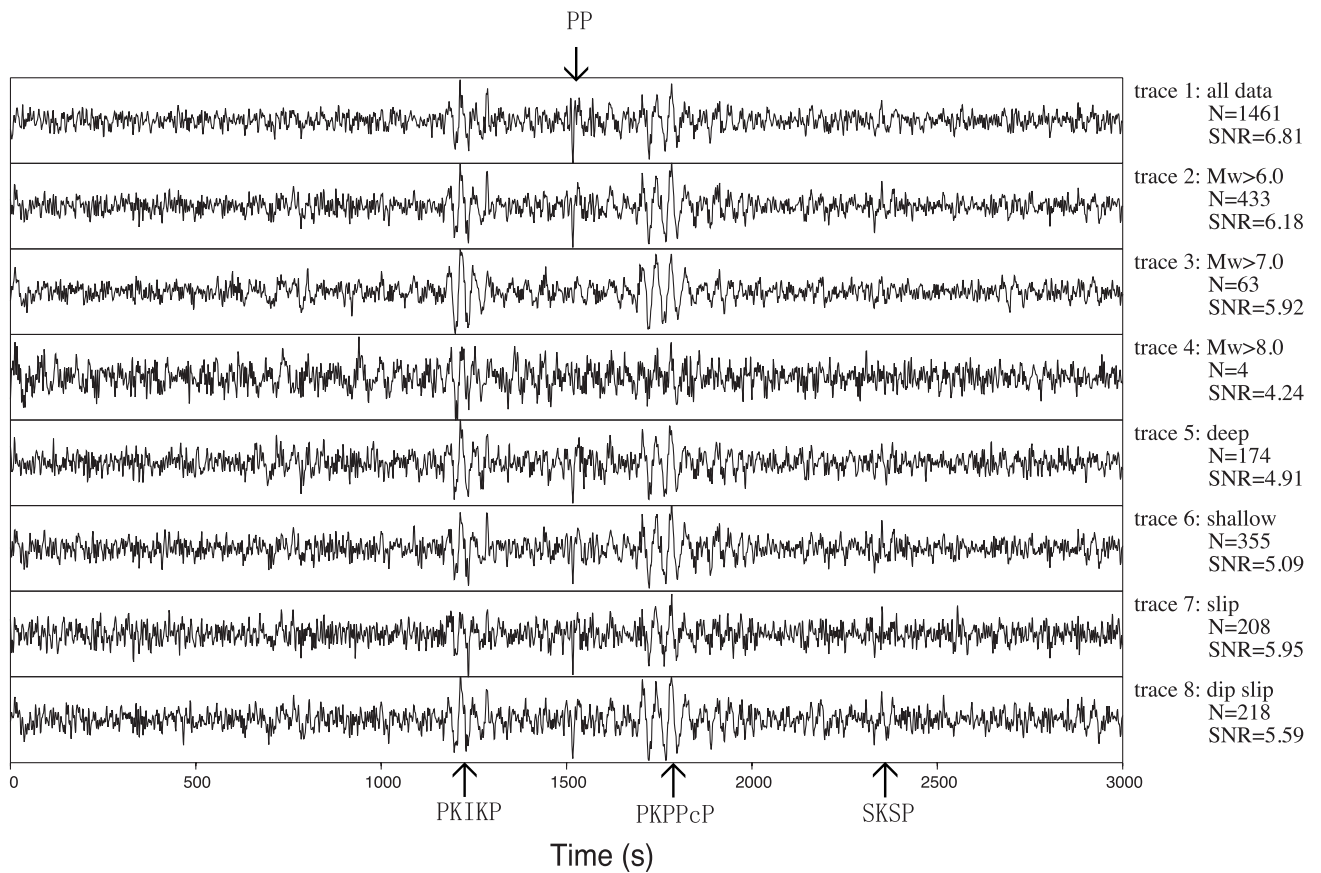


**Figure 5.** Tests of different data selection criteria on stacked EGFs, which used station pairs (a total of 607 pairs) with distances between  $170^\circ$  and  $170.5^\circ$ . Traces 1, 2, 3 and 4 show results by stacking days when there are earthquakes above a certain magnitude (all days without any magnitude threshold,  $M_w \geq 6.0$ ,  $M_w \geq 7.0$  and  $M_w \geq 8.0$ , respectively). Traces 5, 6, 7 and 8 are stacks for days when there are strike-slip, dip-slip, deep-focus (depth  $\geq 50$  km) and shallow ( $< 50$  km) earthquakes, respectively. The label  $N$  means the number of the days used in the stacks. The signal-to-noise ratio (SNR) is measured with respect to the PKIKP phase.

### 3.2.2 Earthquake coda time window and magnitude threshold

We demonstrated above that the triplicated PKP phases can be extracted successfully from noise correlations. Furthermore the main source of the correlations seems to come from earthquake coda energy. Below we explore earthquake coda time windows and magnitude thresholds that may improve the EGF SNRs. We limit the station pairs with azimuths between  $30^\circ$  and  $110^\circ$  and distances between  $170^\circ$  and  $170.5^\circ$ . We use only earthquakes with  $M_w \geq 7.0$  from January to December 2008. Among the dense station pairs, we select only 25 station pairs (randomly). However, the exact same pairs are used for the EGF stacks in these tests. The limited number of station pairs makes it easier to distinguish visually the improvement to deterioration of signal quality in the stacks.

Our tests show that earthquake coda time-window lengths are important for the retrieval of the PKP phase (Fig. 7). It is difficult to extract the body waves from a short coda window (less than 10 000 s, trace 1 and trace 2 in Fig. 7). The SNR (7.26) using coda window 10 000–40 000 s is significantly better than the SNR (5.71) using coda window 10 000–30 000 s. However, when the coda window extends to 10 000–50 000 s, the SNR decreases to 7.02. Thus, the optimal window is around 10 000–40 000 s. The value is similar to that of Lin & Tsai (2013) (around 10 000 to 30 000 s),

which uses  $PcPPKP$  (the strongest phase) to determine the EGF quality.

We also tested effect of different earthquake magnitudes on the signal quality (Fig. 8). The results show that when the magnitude threshold is  $M_w$  6.8 or 6.9, the PKP signal is best (SNR around 6.22 to 6.37). If the magnitude threshold is higher, the number of earthquake decreases, even though the coda energy is greater. If the threshold is lower, even though the number of earthquake increases, the coda energy of the smaller events is too weak to contribute to the SNR.

### 3.2.3 Influence of noise sources on different branches of PKP

Although multiple branches of PKP are clear in the EGF stacks with continuous data (Figs 3 and 4), the later branch of PKP (AB branch) is not obvious in our tests using earthquake coda (Figs 7 and 8). We examine in more details the generation of PKP waves from continuous ambient noise and earthquake coda and the influence of frequency filtering. We choose the interstation distance range of  $157^\circ$ – $157.5^\circ$ , where three branches (df, bc and ab) are expected and relatively separated. We tested three data sets: (1) all the continuous data, (2) continuous data but excluding the days when there is at least one earthquake with  $M_w \geq 6.0$  and (3) coda of earthquakes

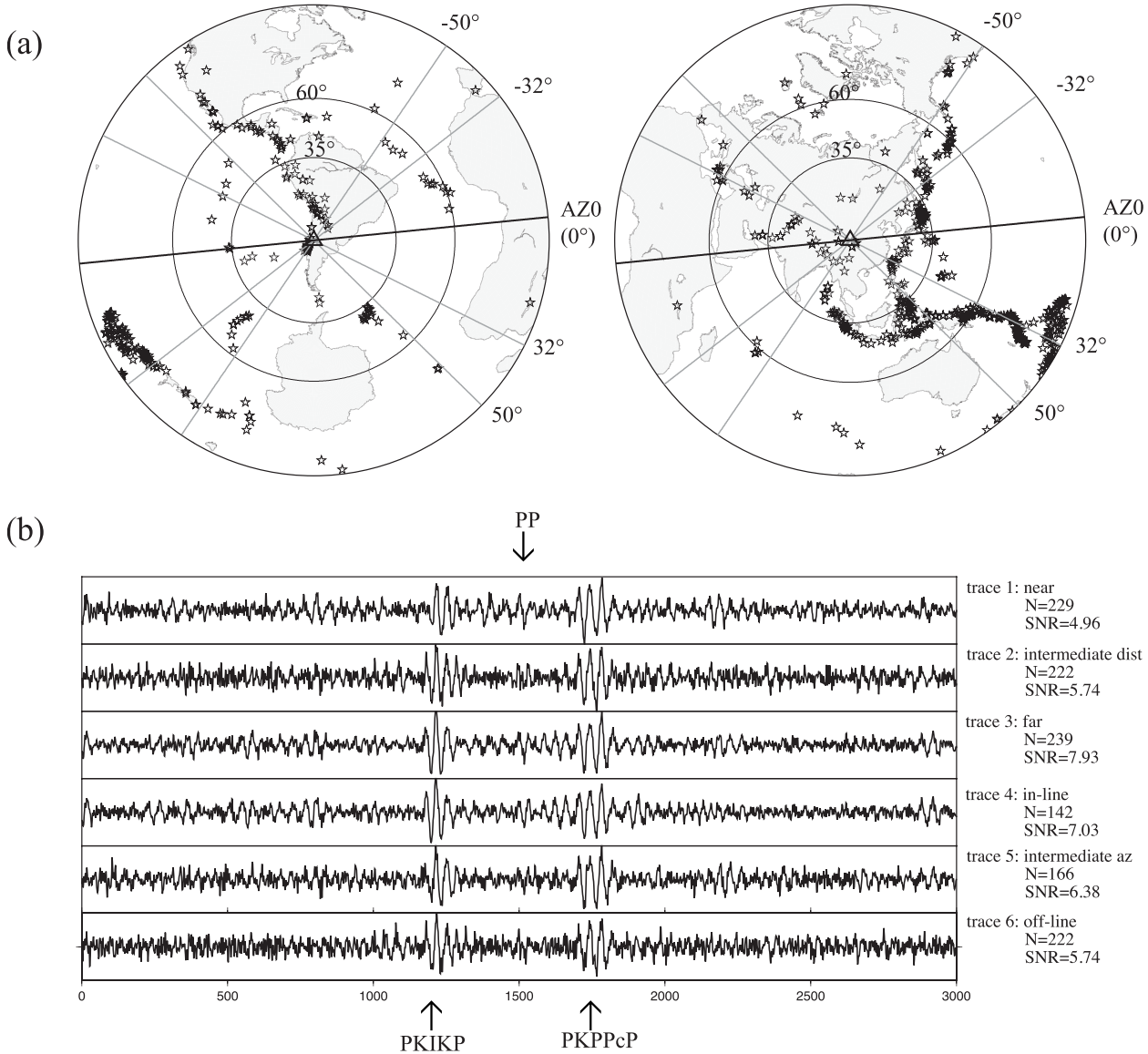


**Figure 6.** Tests of earthquake locations on stacked EGFs from coda correlations. The tests used station pairs (a total of 607 pairs) with distances between  $170^\circ$  and  $170.5^\circ$  (same as in Fig. 5). (a) Maps of earthquakes ( $M_w \geq 6.0$ , black stars) used in the tests. The centres of the stations in SA and China are black triangles in the left and right panels, respectively. The concentric circles indicate distances from the centre ( $35^\circ$ ,  $60^\circ$  and  $90^\circ$ , respectively). The azimuth from the SA centre to the centre in China is  $84.4^\circ$  (AZ0, black thick lines). A few azimuths relative to AZ0 are labelled. (b) Traces 1, 2 and 3 are stacks for earthquakes which are located at near distances ( $\leq 35^\circ$ , inside of smaller circles in Fig. 6a), at intermediate distances ( $> 35^\circ$  and  $\leq 60^\circ$ , between smaller circles and bigger circles in Fig. 6a) and far from the stations ( $\geq 60^\circ$ , outside of bigger circles in Fig. 6a). Traces 4, 5 and 6 use earthquakes at intermediate and large distances ( $> 35^\circ$ ) that are ‘in-line’ with the SA and China arrays (azimuths  $< 32^\circ$  relative to AZ0 or its opposite direction in Fig. 6a), at intermediate azimuths ( $32^\circ$ – $50^\circ$ ) and ‘off-line’ ( $> 50^\circ$ ), respectively. The label  $N$  indicates the number of the events used in the corresponding stack.

$M_w \geq 7.0$  (we use the same coda window as in previous tests for consistency, 10 000 to 30 000 s after the origin time, even though the coda window 10 000 to 40 000 s seems more optimal). The second data set may be considered as the ‘ambient noise’ data devoid of large earthquakes. We applied three separate filters before computing the cross-correlations: ‘broad-band’ filter (periods 5–50 s), ‘shorter-period’ filter (5–20 s) and ‘longer-period’ filter (15–50 s).

From Fig. 9, we summarize the test results in Table 1. At shorter periods, all three branches of PKP can be retrieved from ambient noise (Fig. 9b, top two traces). The ab phase is clearly visible from

earthquake coda, but df and bc phases cannot be observed (Fig. 9b, bottom). At longer periods, the df branch can be retrieved from coda, however, the ab branch is rather weak (Fig. 9c, bottom); signals from ambient noise for any of the branches are rather weak (Fig. 9c, middle). At the broad-band, the EGF waveforms from ambient noise and earthquake coda are significantly different (Fig. 9a, middle and bottom, respectively), resulted from the different behaviours of the phases at different periods. The waveform using all the continuous data (Fig. 9a, top), also showing three PKP branches, is more similar to that from ambient noise than that from the coda.

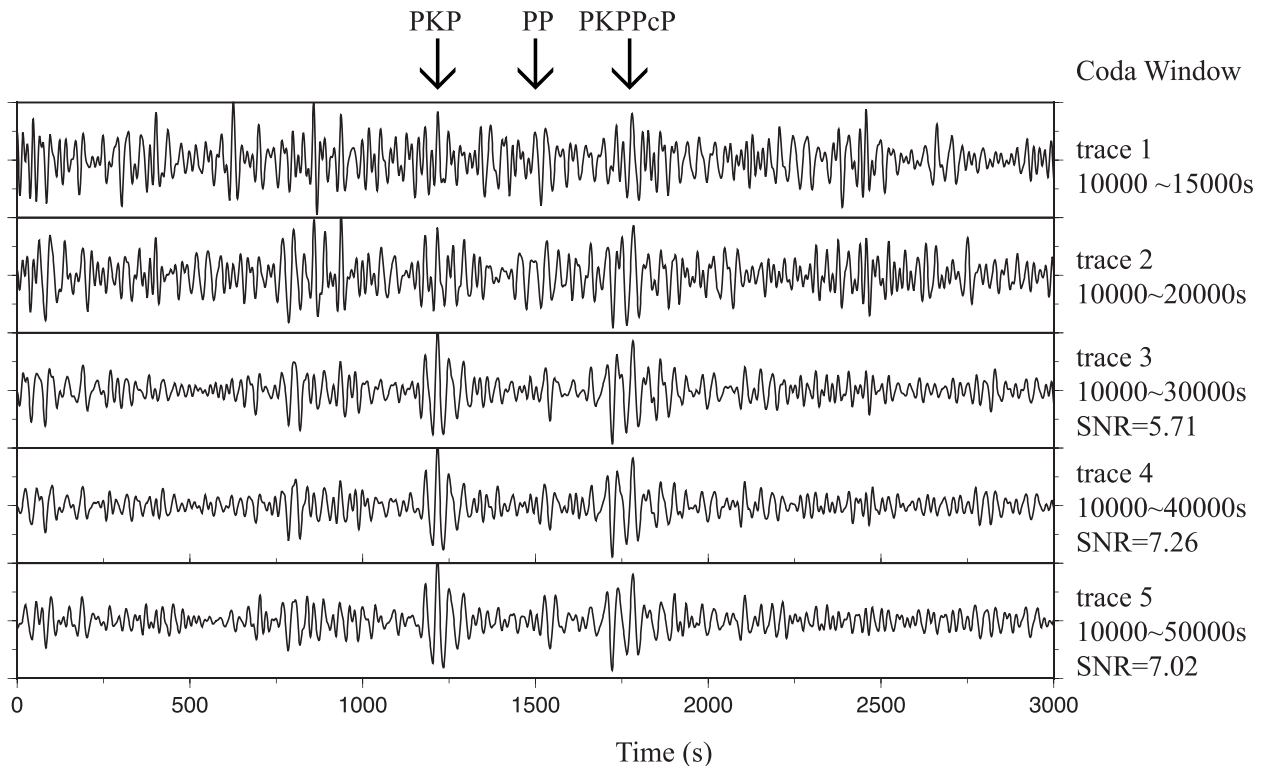


**Figure 7.** Tests of coda window (labelled) on EGFs (traces). We used 25 randomly selected station pairs that have azimuths between  $30^\circ$  and  $110^\circ$  and distances between  $170^\circ$  and  $170.5^\circ$ . We then obtained the stacked EGFs using the coda from the earthquakes from January to December 2008 with  $M_w \geq 7.0$ . The coda window is relative to the origin time of the earthquake.

In summary, both ambient noise and earthquake coda contribute to PKP phases. The contributions vary with frequency and with body-wave phases. At shorter periods (5–20 s), three branches of PKP (df, bc and ab) can be extracted from ambient noise and ab phase from earthquake coda. At longer periods (15–50 s), earthquake-coda wave is effective in generating the df branch, but not the ab branch; ambient noise is not effective in generating any of the branches.

The different behaviours are probably related to the nature of the two types of noise sources. The ambient noise is dominated by shorter periods (less than 10 s) in spectrum, while major earthquakes are dominated by longer-periods and the coda has rich longer-period energy than the ambient noise (Fig. 10). The spectral difference can explain the observed variation of the PKP phases with frequency. However, for coda waves, the different branches of PKP (with slightly different ray parameters) are highly variable, which may suggest that the noise field generated by the coda of limited number of major earthquakes is less ‘diffuse’ than by the ambient noise source. However, given the limited length of the coda window and the limited number of major earthquakes needed, coda waves are much more effective in generating certain body waves than the ambient noise, such as PKP<sub>df</sub> phase here or PKIKP<sup>2</sup> and PKIKP phases in Wang *et al.* (2015).

#### 4 CONCLUSION AND DISCUSSION

We report observations of triplicated PKP phases from stacks of station–station noise correlations. Three branches of PKP (df, bc

and ab) can be observed from distances around  $150^\circ$  to  $160^\circ$ , and two branches (df and ab) can be observed continuously to  $180^\circ$ . Both ambient noise and earthquake coda contribute to the PKP phases. However, the contributions vary with frequency and with the branches of the PKP. At shorter periods (5–20 s), three branches of PKP (df, bc and ab) can be extracted from ambient noise and ab phase from earthquake coda. At longer periods (15–50 s), earthquake coda are effective in generating the df branch, but not the ab branch. Comparing contributions of ambient noise and earthquake coda to the PKIKP phase (df branch) at the broad-band (5–50 s), the coda of large earthquakes is the major source energy in the noise correlations. The location of the earthquakes has great influences on the SNR of the PKIKP phase. Earthquakes far from the stations and in-line with station pairs contribute more to the convergence of the body waves. In the meanwhile, different depths and mechanism of earthquakes do not affect significantly the results of the correlations. The best coda window is around 10 000–40 000 s after the earthquake occurrence and the best threshold magnitude of earthquakes is  $M_w \geq 6.8$  or 6.9 in generating the PKIKP phase.

Our results, with special emphases on PKP phases, suggest that both proposals on the sources generating the body waves are valid, that is, the coda of large earthquakes (Lin & Tsai 2013; Lin *et al.* 2013) or the ambient noise (Boué *et al.* 2013; Nishida 2013). The body-wave generation depends on frequency and phases, as we have shown with PKP waves. The frequency dependence of the emergence of body waves is consistent with Boué *et al.* (2014), which suggests that the long-period signals may come from earthquake reverberations while short-period signals may come from scattering. When a phase can be generated by both ambient noise and coda

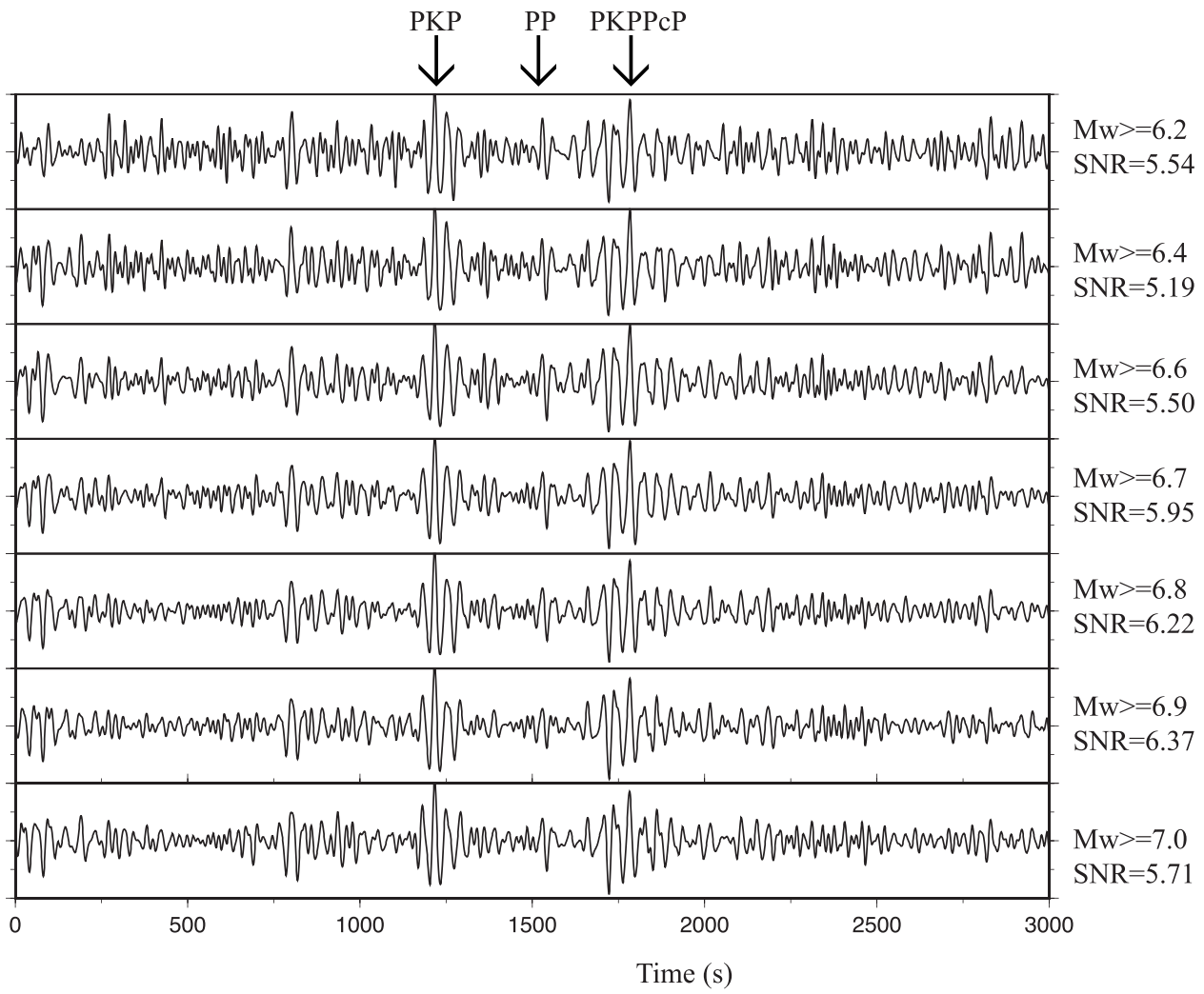


**Figure 8.** Tests of magnitude threshold (labelled) on EGFs (traces). The data used were same as in Fig. 7. The coda window was 10 000–30 000 s.

energy (e.g. PKIKP at broad-band), earthquake coda are much more effective.

The fact that some body-wave phases are better extracted from noise correlations than others are well demonstrated in previous studies (Boué *et al.* 2013; Lin *et al.* 2013; Lin & Tsai 2013; Nishida 2013). In Fig. 5, we can observe other examples of body-wave variability in PP and SKP phases, which are not visible in traces 3 and 4 (when only segments of major earthquakes were used). Nevertheless, because of the similarity in their ray parameters and ray paths, it is surprising to observe the different behaviours of PKP(df) and PKP(ab) in this study with respect to noise sources (ambient noise or earthquake coda) and frequency. On the other hand, the different behaviours offer interesting opportunities to enhance individual arrivals (df and ab phases in this case) separately, which can still be combined to analyse relative times because they are related to the same station pairs. The causes for the different behaviours with respect to noise sources, seismic body-wave phases and frequencies need to be investigated in the future.

The observation of triplicated PKP branches from noise provides a new type of data for studying the Earth's core, in particularly the inner core. Traditional observations of PKP waveforms from earth-

quakes come mostly from subduction zones, which are quite limited geographically. The new type of data provides vastly different coverage from stations across the continents and, because the station locations are precisely known, the new data are not affected by source location errors while body waves from earthquakes would. The application of this new type of observations has recently been demonstrated by the autocorrelation study of Wang *et al.* (2015), which achieves fairly uniform global coverage of the PKIKP<sup>2</sup> rays going through the very centre of the Earth. For PKP waves, stations in high latitudes in northern hemisphere and those in Antarctica would provide immediately new polar paths for constraining the inner core anisotropy.

## ACKNOWLEDGEMENTS

The waveform data of the China Regional Seismic Networks were provided from the Data Management Centre of China National Seismic Network at Institute of Geophysics, China Earthquake Administration (Zheng *et al.* 2009); other station data were obtained from the IRIS DMC. We thank reviews from Victor Tsai and an anonymous reviewer. Most figures were plotted using the GMT

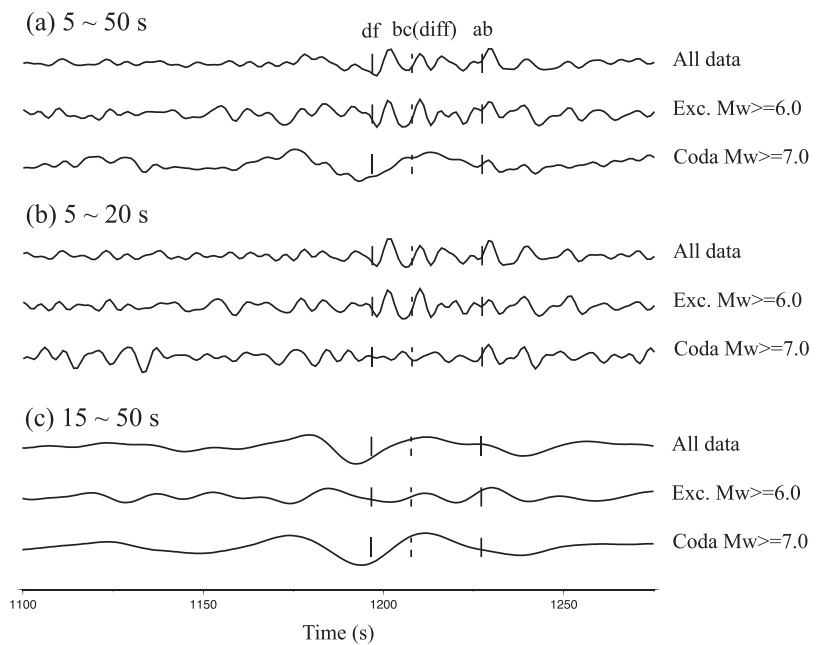


**Figure 9** EGFs from interstation cross-correlations stacking using different original data and bandpass filters (5–50, 5–20, 15–50 s). The original data include the continuous data of all the available days, the continuous data that exclude the days containing strong earthquakes ( $M_w \geq 6.0$ ) and only the coda of major earthquakes ( $M_w \geq 7.0$ ). The traces are stacks of the same station pairs with distances from  $157^\circ$  to  $157.5^\circ$ . The theoretical arrival times (black lines) are calculated from the IASP91 model.

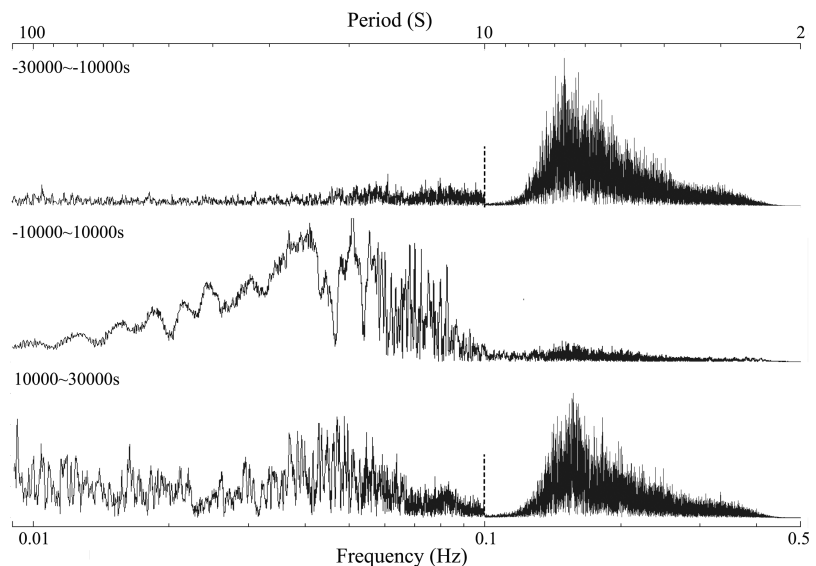


**Figure 10.** Typical spectra before (top), during (middle) and after (bottom) a major earthquake. This example is  $M_w$  7.0 on 2008-6-30 6:17:43 at  $53.88^\circ\text{N}$   $152.89^\circ\text{E}$  recorded at station ZL.REGU in South America. The portion at periods longer than 10 s (dashed lines) at top and bottom are enlarged by five times for better visualization.

**Table 1.** PKP branches that can be extracted from noise correlations.<sup>a</sup>

Noise source	Short periods (5–20 s)	Long periods (15–50 s)	Broad-band (5–50)
Ambient noise	df, bc, ab	all weak	df, bc, ab
Earthquake coda	ab	df, bc(?)	df, bc(?), weak ab

<sup>a</sup>Question mark indicates uncertainty in the observation.

software (Wessel & Smith 1991). This work was supported by the Ministry of Science and Technology of China (2014CB845901), the Natural Science Foundation of China (41330209) and the US National Science Foundation (EAR 1215824).

## REFERENCES

- Bensen, G.D., Ritzwoller, M.H., Barmin, M.P., Levshin, A.L., Lin, F., Moschetti, M.P., Shapiro, N.M. & Yang, Y., 2007. Processing seismic ambient noise data to obtain reliable broad band surface wave dispersion measurements, *Geophys. J. Int.*, **169**, 1239–1260.
- Boué, P., Poli, P., Campillo, M., Pedersen, H., Briand, X. & Roux, P., 2013. Teleseismic correlations of ambient seismic noise for deep global imaging of the Earth, *Geophys. J. Int.*, **194**(2), 844–848.
- Boué, P., Poli, P., Campillo, M. & Roux, P., 2014. Reverberations, coda waves and ambient noise: correlations at the global scale and retrieval of the deep phases, *Earth planet. Sci. Lett.*, **391**, 137–145.
- Campillo, M. & Paul, A., 2003. Long-range correlations in the diffuse seismic coda, *Science*, **299**(5606), 547–549.

- Cao, A., Masson, Y. & Romanowicz, B., 2007. Short wavelength topography on the inner-core boundary, *Proc. Natl. Acad. Sci. USA*, **104**(1), 31–35.
- Cormier, V.F., Xu, L. & Choy, G.L., 1998. Seismic attenuation of the inner core: viscoelastic or stratigraphic?, *Geophys. Res. Lett.*, **25**(21), 4019–4022.
- Creager, K.C., 1992. Anisotropy of the inner core from differential traveltimes of the phases PKP and PKIKP, *Nature*, **356**, 309–314.
- Irving, J.C.E. & Deuss, A., 2011. Hemispherical structure in inner core velocity anisotropy, *J. geophys. Res.*, **116**, B04307, doi:10.1029/2010JB007942.
- Ishii, M. & Dziewoński, A.M., 2002. The innermost inner core of the Earth: Evidence for a change in anisotropic behavior at the radius of about 300 km, *Proc. Natl. Acad. Sci. USA*, **99**(22), 14 026–14 030.
- Lin, F.C. & Tsai, V.C., 2013. Seismic interferometry with antipodal station pairs, *Geophys. Res. Lett.*, **40**, 4609–4613.
- Lin, F.C., Tsai, V.C., Schmandt, B., Duputel, Z. & Zhan, Z., 2013. Extracting seismic core phases with array interferometry, *Geophys. Res. Lett.*, **40**, 1049–1053.
- Lobkis, O.I. & Weaver, R.L., 2001. On the emergence of the Green's function in the correlations of a diffuse field, *J. acoust. Soc. Am.*, **110**, 3011–3017.
- Kennett, B.N. & Engdahl, E., 1991. Traveltimes for global earthquake location and phase identification, *Geophys. J. Int.*, **105**(2), 429–465.
- Nishida, K., 2013. Global propagation of body waves revealed by cross-correlation analysis of seismic hum, *Geophys. Res. Lett.*, **40**, 1691–1696.
- Niu, F.L. & Wen, L.X., 2001. Hemispherical variations in seismic velocity at the top of the Earth's inner core, *Nature*, **410**, 1081–1084.
- Poli, P., Campillo, M. & Pedersen, H. & LAPNET Working Group, 2012. Body-Wave Imaging of Earth's Mantle Discontinuities from Ambient Seismic Noise, *Science*, **338**, 1063–1065.
- Roux, P., Sabra, K.G., Gerstoft, P., Kuperman, W.A. & Fehler, M.C., 2005. P-waves from cross-correlation of seismic noise, *Geophys. Res. Lett.*, **32**, L19393, doi:10.1029/2005GL023803.
- Sens-Schönfelder, C., Snieder, R. & Stähler, S.C., 2015. The lack of equipartitioning in global body wave coda, *Geophys. Res. Lett.*, **42**(18), 7483–7489.
- Shapiro, N.M. & Campillo, M., 2004. Emergence of broadband Rayleigh waves from correlations of the ambient seismic noise, *Geophys. Res. Lett.*, **31**, L07614, doi:10.1029/2004GL019491.
- Shapiro, N.M., Campillo, M., Stehly, L. & Ritzwoller, M.H., 2005. High resolution surface wave tomography from ambient seismic noise, *Science*, **307**, 1615–1618.
- Shearer, P.M. & Toy, K.M., 1991. PKP (BC) versus PKP (DF) differential travel times and aspherical structure in the Earth's inner core, *J. geophys. Res.*, **96**(B2), 2233–2247.
- Song, X.D. & Helmberger, D.V., 1993. Anisotropy of the Earth's inner core, *Geophys. Res. Lett.*, **20**, 2591–2594.
- Song, X.D. & Dai, W., 2008. Topography of Earth's inner core boundary from high-quality waveform doublets, *Geophys. J. Int.*, **175**, 386–399.
- Song, X.D. & Richards, P.G., 1996. Seismological evidence for differential rotation of the Earth's inner core, *Nature*, **382**, 221–224.
- Sun, X.L. & Song, X.D., 2008a. Tomographic inversion for three-dimensional anisotropy of Earth's inner core, *Phys. Earth. planet. Inter.*, **167**, 53–70.
- Sun, X.L. & Song, X.D., 2008b. The inner inner core of the Earth: texturing of iron crystals from three-dimensional seismic anisotropy, *Earth planet. Sci. Lett.*, **269**, 56–65.
- Tanaka, S. & Hamaguchi, H., 1997. Degree one heterogeneity and hemispherical variation of anisotropy in the inner core from PKP(BC)-PKP(DF)times, *J. geophys. Res.*, **102**, 2925–2938.
- Vidale, J.E., Dodge, D.A. & Earle, P.S., 2000. Slow differential rotation of the Earth's inner core indicated by temporal changes in scattering, *Nature*, **405**, 445–448.
- Wang, T., Song, X.D. & Xia, H. H., 2015. Equatorial anisotropy in the inner part of Earth's inner core from autocorrelation of earthquake coda, *Nat. Geosci.*, **8**(3), 224–227.
- Wen, L.X., 2006. Localized temporal change of the Earth's inner core boundary, *Science*, **314**, 967–970.
- Wessel, P. & Smith, W. H., 1991. Free software helps map and display data, *EOS, Trans. Am. geophys. Un.*, **72**(41), 441–446.
- Yao, H., van der Hilst, R.D. & de Hoop, M.V., 2006. Surface-wave array tomography in SE Tibet from ambient seismic noise and two-station analysis—I. Phase velocity maps, *Geophys. J. Int.*, **166**, 732–744.
- Zhan, Z., Ni, S., Helmberger, D. & Clayton, R., 2010. Retrieval of Moho-reflected shear wave arrivals from ambient seismic noise, *Geophys. J. Int.*, **182**, 408–420.
- Zhang, J., Song, X., Li, Y., Richards, P.G., Sun, X. & Waldhauser, F., 2005. Inner core differential motion confirmed by earthquake waveform doublets, *Science*, **309**, 1357–1360.
- Zheng, S., Sun, X., Song, X., Yang, Y. & Ritzwoller, M.H., 2008. Surface wave tomography of China from ambient seismic noise correlation, *Geochem. Geophys. Geosyst.*, **9**, Q0502, doi:10.1029/2008GC001981.
- Zheng, X.F., Ouyang, B., Zhang, D.N., Yao, Z.X., Liang, J.H. & Zheng, J., 2009. Technical system construction of Data Backup Centre for China Seismograph Network and the data support to researches on the Wenchuan earthquake, *Chin. J. Geophys.*, **52**(5), 1412–1417.